Since January 2020 Elsevier has created a COVID-19 resource centre with free information in English and Mandarin on the novel coronavirus COVID-19. The COVID-19 resource centre is hosted on Elsevier Connect, the company's public news and information website.

Journal of Electroanalytical Chemistry 894 (2021) 115341

Contents lists available at ScienceDirect

Journal of Electroanalytical Chemistry

journal homepage: www.elsevier.com/locate/jelechem

Ultra-precise label-free nanosensor based on integrated graphene with Au nanostars toward direct detection of IgG antibodies of SARS-CoV-2 in blood

Seyyed Alireza Hashemi [a,*,1], Sonia Bahrani [b,1], Seyyed Mojtaba Mousavi [c,1], Navid Omidifar [d,e,*], Nader Ghaleh Golab Behbahan [f], Mohammad Arjmand [a,*], Seeram Ramakrishna [g,*], Kamran Bagheri Lankarani [b], Mohsen Moghadami [b], Mansoureh Shokripour [d], Mohammad Firoozsani [h], Wei-Hung Chiang [c]

[a] Nanomaterials and Polymer Nanocomposites Laboratory, School of Engineering, University of British Columbia, Kelowna, BC V1V 1V7, Canada
[b] Health Policy Research Center, Health Institute, Shiraz University of Medical Sciences, Shiraz, Iran
[c] Department of Chemical Engineering, National Taiwan University of Science and Technology, Taiwan
[d] Department of Pathology, School of Medicine, Shiraz University of Medical Sciences, Shiraz, Iran
[e] Clinical Education Research Center, Shiraz University of Medical Sciences, Shiraz, Iran
[f] Department of Poultry Diseases, Razi Vaccine and Serum Research Institute, Agricultural Research, Education and Extension Organization (AREEO), Shiraz Branch, Shiraz, Iran
[g] Center for Nanofibers and Nanotechnology, National University of Singapore, Singapore
[h] Member of Board of Trustees, Zand Institute of Higher Education, Shiraz, Iran

ARTICLE INFO

Keywords:
SARS-CoV-2
COVID-19
Coronavirus
Nanosensor
Antibody

ABSTRACT

Rapid distribution of airborne contagious pathogenic viruses such as SRAS-CoV-2 and their severely adverse impacts on different aspects of the human society, along with significant weaknesses of traditional diagnostic platforms, raised the global requirement for the design/fabrication of precise, sensitive, and rapid nanosystems capable of specific detection of viral illnesses with almost negligible false-negative results. To address this indispensable requirement, we have developed an ultra-precise fast diagnostic platform capable of detecting the trace of monoclonal IgG antibody against S1 protein of SARS-CoV-2 within infected patients' blood specimens with COVID-19 in about 1 min. The as-developed electrochemical-based nanosensor consists of a highly activated graphene-based platform in conjunction with Au nanostars, which can detect SARS-CoV-2 antibodies with a fantastic detection limit (DL) and sensitivity of 0.18×10^{-19}%V/V and 2.14 μA.%V/V.cm^{-2}, respectively, in human blood plasma specimens even upon the presence of a high amount of interfering compound/antibodies. The nanosensor also exhibited remarkable sensitivity/specificity compared with the gold standard (i.e., ELISA assay), which furtherly confirmed its superb performance.

1. Introduction

Rapid distribution of airborne pathogenic viruses throughout the world and their subsequent vast mortality in different countries raised global demand for the design/development of efficient, reliable, and rapid diagnostic kits to detect pathogenic viruses within biological fluids to stop their fast person-to-person transferring chain. Among these viruses, SARS-CoV-2, viz., severe acute respiratory syndrome coronavirus 2, is a nano-sized (about 100 nm) enveloped-based positively sense single genomic stranded RNA crown-shaped virus that can rapidly transfer among people through close interaction and spilled respirational compounds, e.g., sneeze or cough, which is also known as a highly infectious airborne virus from beta coronaviruses' family [1–4].

Coronaviruses are a vast family of pathogenic viruses that contain different categories and cause mild/moderate upper respiratory tract illness, e.g., common cold [5]. So far, seven types of coronaviruses have been identified that can infect human being where four of them, i.e., 229E, NL63, OC43 and HKU1, are responsible for one-third of common flu throughout the world and can only cause mild illnesses, while the rest of them can cause severe sicknesses among which SARS-CoV, MERS-CoV, and SARS-CoV-2 can be mentioned [6]. Correspondingly, SARS-CoV-2 showed less mortality compared with SARS-CoV (10%) and MERS-CoV (35%); however, it showed superiorly

* Corresponding authors at: Department of Pathology, School of Medicine, Shiraz University of Medical Sciences, Shiraz, Iran (N. Omidifar).
E-mail addresses: sa_hashemi@sums.ac.ir (S. Alireza Hashemi), omidifarn@sums.ac.ir (N. Omidifar), mohammad.arjmand@ubc.ca (M. Arjmand), seeram@nus.edu.sg (S. Ramakrishna).
[1] These authors have equal contributions in the preparation of this manuscript and accomplishing experimental works.

https://doi.org/10.1016/j.jelechem.2021.115341
Received 4 February 2021; Received in revised form 11 April 2021; Accepted 5 May 2021
Available online 8 May 2021

higher infectivity and transmissibility [6,7]. Moreover, SARS-CoV-2 exhibits different signs in people that range from mild symptoms to life-threatening situations [8]. In this regard, most people only show flu-like symptoms, while the rest of them experience more severe symptoms such as thrombophilic vasculitis in the lung and interstitial pneumonia [9].

Since the announcement of the SARS-CoV-2 pandemic [10], the lack of specific, sensitive, and rapid diagnostic kits has become a significant pitfall toward stopping the transfer chain of SARS-CoV-2. The major point for controlling a viral pandemic is wise isolation of suspected or ill people via strict quarantine strategies, which require practical tools such as ultra-sensitive/specific, rapid, and reliable diagnostic kits. In this matter, there are two main methods for the detection of viral infections, among which detection of nucleic acid (i.e., RNA or DNA) and viral biomarkers (i.e., antibodies and antigens) can be mentioned [11,12]. Among the methods discussed above, RT-PCR and enzyme-linked immunosorbent assay (ELISA) is the most well-known procedures for direct detection of either nucleic acids or antigen/antibody within biological fluids. These traditional methods suffer some demerits such as the requirement for extraction, viral isolation, a sophisticated laboratory, high rate of false-negative, well-trained personnel and time-consuming processes, which are not compatible with the fast transferring rate of SARS-CoV-2 and cannot render the possibility for rapid isolation of infected people [13]. Therefore, developing a quick, precise, and sensitive sensor for specific detection of viruses within biological media is crucial.

Biosensors are the key to this urgent demand. They could be considered a valid alternative instead of traditional flawful methods due to their excellent sensitivity/specificity that offers a rapid manner for detecting pathogenic viruses. Biosensors can be classified into several subgroups, including antigen/antibody-based, nucleic acid-based, enzymatic, and whole cell-based biosensors [14]. Owing to the urgency of COVID-19, researchers worldwide conducted great efforts to develop state-of-the-art biosensors for the fast identification of SARS-CoV-2 in biological specimens. Among recently developed platforms, field-effect transistor-based immunosensor coupled with SARS-CoV-2 spike antibody with a detection limit (DL) of 2.42×10^2 copies.mL^{-1} [15], an electrochemical impedance-based immune biosensor for identification of SARS-CoV-2 antibody [16], ACE-2 receptor-based lateral flow immunoassay (LFIA) for detection of Spike 1 protein of SARS-CoV-2 with DL of 1.86×10^5 copies.mL^{-1} [17], an electrochemical assay based on decorated calixarene functionalized graphene oxide (GO) toward detecting SARS-CoV-2 RNA with DL of 200 copies.mL^{-1} [18], detection of induced reactive oxygen species (ROS) related to lung/respiratory epithelium of infected people with COVID-19 [19] and immunosensor based on the carbon black integrated magnetic beads toward detection of S and N proteins of SARS-CoV-2 within saliva samples with DL of 19 and 8 ng.mL^{-1}, respectively [20], can be mentioned. What is more, in a work by Torrente-Rodrı´guez et al. [21], they developed a graphene-based multiplexed economic rapid diagnostic kit that can simultaneously detect nucleocapsid protein of viral antigen, IgG/IgM antibodies and C-reactive protein as an inflammatory biomarker; the developed platform can be used as an ultrasensitive and rapid detection approach for accurate identification of SARS-CoV-2 and its related biomarkers within biological fluids, which showed remarkable performance as a multiplex detection platform. These works highlight the superiority of the new generation of biosensors over traditional detection platforms, viz., RT-PCR and ELISA, toward fast and precise tracking of pathogenic viruses or their biomarkers within biological specimens.

Despite all of the progress, developed biosensors use biological markers that provide them with limited sensitivity and DL, while a majority of them cannot identify infected people at either incubation or prodromal period of the disease. In our previous work, for the first time, we have developed a rapid label-free graphene-based nanosensor that can detect the trace of SARS-CoV-2 in about 1 min based on the applied step potential without any biological receptor within different biological fluids (i.e., swab, saliva and blood) with significantly low DL and great sensitivity of about 1.68×10^{-22} μg.mL^{-1} and 0.0048 μA.μg.mL^{-1}.cm^{-2}, respectively. The as-developed nanosensor can also be used as a viral characterization approach and detect different viruses' fingerprints through their differentiable specific electrochemical patterns at vividly different voltage positions within any biological and non-biological fluids [22].

Herein, we have developed an improved label-free nanosensor composed of activated graphene oxide (GO) in conjunction with Au nanostars (Au NS) (G-Au NS) toward direct detection of the monoclonal IgM antibodies against S1 glycoprotein of SARS-CoV-2 within blood specimens of infected or suspected people with the infectious disease of COVID-19. The activated graphene oxide is composed of 8-hydroxyquinoline (8H), 1-ethyl-3-(3-dimethylaminopropyl), carbodiimide (EDC) and *N*-hydroxysuccinimide (NHS). Correspondingly, developed nanosensors were well-characterized and used for enhancement of glassy carbon electrode (GCE) and working electrode of DRP C110 carbon-based screen-printed electrode. Then, the obtained data were compared with the ELISA assay as the gold standard to evaluate the performance of developed nanosensors toward label-free detection of monoclonal IgG antibodies against S1 glycoprotein of SARS-CoV-2 as confident COVID-19 detection metrics.

2. 2.Results and discussion

2.1. Characterization of fabricated nanomaterials

In this study, produced nanomaterials were evaluated via different analyses to assess their quality and successful fabrication. Fig. 1 (a) shows that low-angle XRD, i.e., X-ray diffractogram, of well-exfoliated GO is demonstrated. As depicts, obtained GO nanoflakes showed a well-resolved broad peak at 2Θ of 22.8, which correspond to the (0 0 2) plane of GO, whereas the Raman spectrum (Fig. 1 (b)) of GO with D, G and D + G bands peaks at about 1341, 1592 and 2693 cm^{-1} along with I_D/I_G ratio of 0.92 furtherly confirmed the successful fabrication of GO along with its high quality [23].

Moreover, in Fig. 1 (c) (I-III), the FTIR spectrum of GO, activated GO, and Au NS can be seen, respectively. As depicts within part (I), following XRD and Raman spectroscopy results, GO is successfully synthesized with main functional groups such as C—H sp^2 (802 cm^{-1}), in-plane vibration of C—H (1011 cm^{-1}), CO alkoxy (1084 cm^{-1}), unoxidized C═C double bond carbon atoms, which is known as the primary fingerprint of graphene (1565 cm^{-1}), viz., the fingerprint of the heterocyclic structure of graphene flake, carbonyl (i.e., C═O) functional groups (1695 cm^{-1}) and dominant hydrophilic hydroxyl (i.e., –OH) functional groups (3077 cm^{-1}) [22–24]. Correspondingly, in part (II) of Fig. 1, the FTIR spectrum of activated GO is demonstrated. As illustrated, each appeared peak is attributed to the benzene ring of 8H (445 cm^{-1}), torsion of benzene ring related to 8H (608 cm^{-1}), asymmetric out-of-plane –OCN groups related to NHS (675 cm^{-1}), bending of C—H functional group of 8H (742 cm^{-1}), out-of-plane = C—H and = CH_2 groups of 8H decorated on the surface of GO (786 cm^{-1}), out-of-plane deformation of CH_3 related to 8H (820 cm^{-1}), aromatic benzene ring of 8H (960 cm^{-1}), C—H stretching vibration of 8H (1069 cm^{-1}), stretching vibration of –CNC- functional group arose from NHS (1209 cm^{-1}), stretching vibration of O—C group of 8H (1312 cm^{-1}), bending of CH_3 functional group of 8H (1408 cm^{-1}), in-plane deformation of CH_2 group of 8H (1495 cm^{-1}), fingerprint of GO (1564 cm^{-1}), viz., C═C double bond carbon atoms peak, CO amide group of NHS (1646 cm^{-1}), vibration of -C═O groups related to NHS (1717 cm^{-1}), superiorly active -N═C = N- chemical group of EDC (2112 cm^{-1}), –OH functional group (3037 cm^{-1}) and –NH functional group of either NHS or 8H

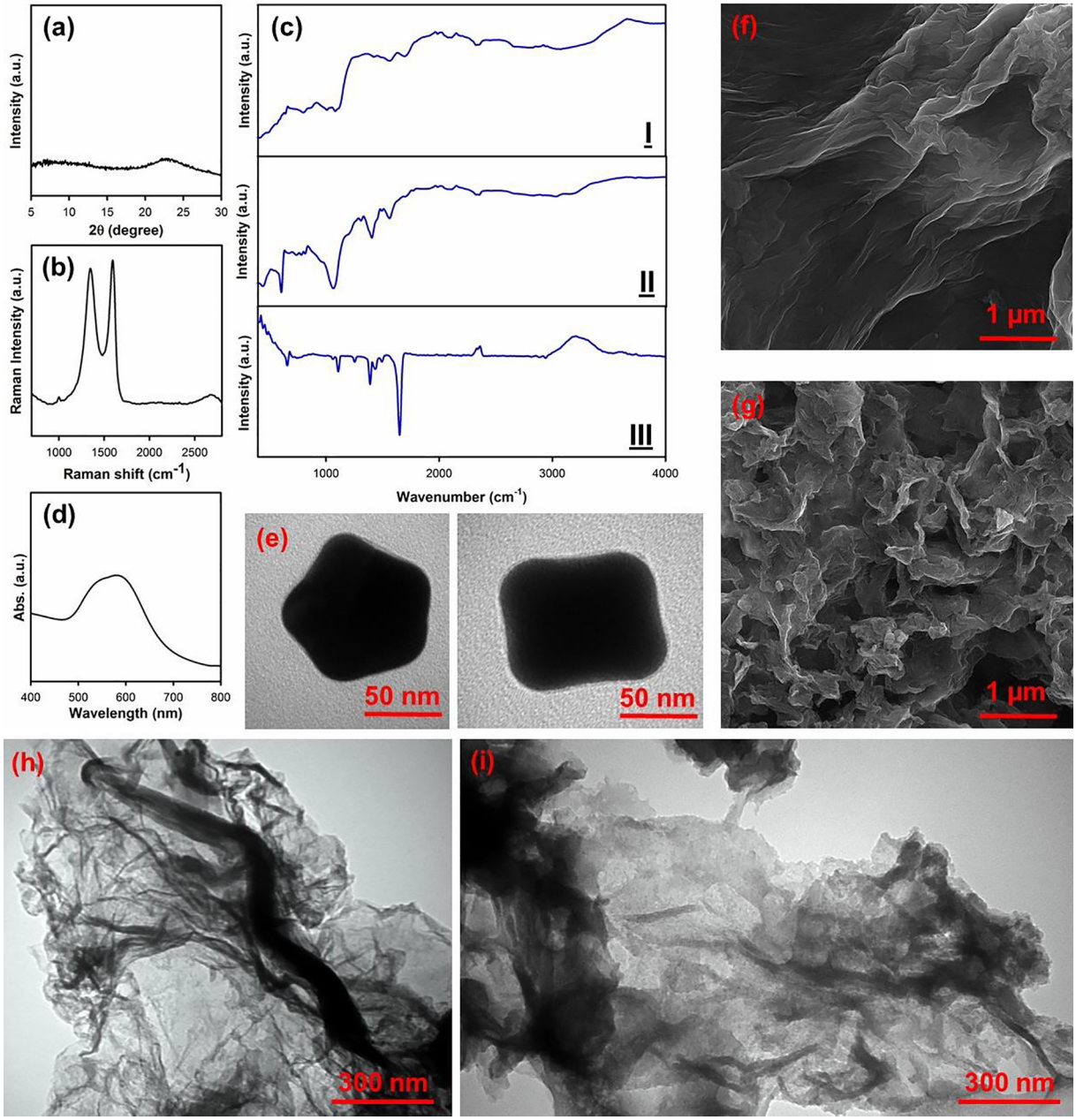

Fig. 1. (a) X-ray diffraction of well-exfoliated GO, (b) Raman spectroscopy result of GO, (c) FTIR spectrums of developed nanomaterials (I) GO, (II) activated GO and (III) Au NS, (d) UV–vis spectroscopy of Au NS, (e) TEM images of Au NS, (f) FESEM image of well-exfoliated GO, (g) FESEM image of activated GO and (h & i) TEM images of activated GO with 300 nm scale bar; in this image, all of the used chemical compounds were characterized separately, and the developed nanosensor is prepared upon adding proper amount of activated GO and Au NSs to the suspension.

(3205 cm^{-1}) [22]. The appearance of these peaks in the FTIR spectrum of the hybrid 2D platform of activated GO highlighted the successful decoration of well-exfoliated GO flakes with main/active functional groups of 8H, EDC and NHS, which considerably enhance the sensitivity of GO for precise detection of monoclonal IgG antibody against S1 glycoprotein of SARS-CoV-2 from its active domains.

In Fig. 1 (c) (III), the FTIR spectrum of Au NSs can be seen. As depicts within this spectrum, Au NSs were successfully fabricated with common functional groups such as N—H functional groups related to primary and secondary amines (657–748 cm^{-1}), the vibration of C—O (1061 cm^{-1}), stretching vibration of C—N functional groups (1108 cm^{-1}), aliphatic amines groups (C—N) (1253 cm^{-1}), banding of O—H groups (1390 cm^{-1}), the vibration of C—H (1433–1494 cm^{-1}), bending of primary amine (N—H) (1649 cm^{-1}), stretching vibration of alkane (C—H) (2938 cm^{-1}) and stretching vibration of O—H as a result of Au^{3+} reduction into Au^{0}. Similarly, the UV–Vis spectroscopy result of Au NS was in accord with its FTIR spectrum and corroborated the successful synthesis of Au NSs. In this regard, the peak at around 575 nm corresponds to the localized surface plasmon resonance (LSRP) mode of an out-of-plane dipole or out-of-plane LSPR [22].

Additionally, in Fig. 1 (e), TEM images of Au NSs can be seen that demonstrate well-resolved star-shaped morphology with size distribution variable from 92 to 105 nm. Besides, FESEM images of GO and activated GO with 8H, EDC and NHS can be seen in Fig. 1 (f) and (g), respectively. As shown in part (f), GO is perfectly exfoliated from pristine graphite and presents a wide/active surface area ideal for modification/activation with desirable functional groups toward

detecting target compounds. Likewise, activated GO also exhibits a 2D planar structure ideal for interaction with antibodies owing to the well-distribution of functional groups of 8H, EDC and NHS all around its basal plane. In Fig. 1 (h & i), TEM images of activated GO can be seen. As depicted, activated GO shows an excellent flake of GO that not only confirms the fantastic exfoliation of GO and formation of single-layer GO but also clearly demonstrates the homogenous distribution of 8H, EDC and NHS related functional groups all around the wide surface area of GO, providing abundant active sites for effective attraction/detection of monoclonal antibodies against S1 glycoproteins.

2.2. Direct electrochemical detection of SARS-CoV-2 IgG antibodies

The electrochemical performance of enhanced electrodes with developed nanomaterials was assessed in $(Fe(CN)_6)^{3-/4-}$ as redox probes through cyclic voltammetry (CV) and EIS analyses, as performed in our previous work [25]. Fig. 2 (a) demonstrates the obtained data from CV analysis for the decorated/modified GCE with Au-NS, activated GO and G-Au NS. The evaluation was conducted in a solution containing 5 mM $(Fe(CN)_6)^{3-/4-}$ and 0.1 M KCl at a scan rate of 100 $mV.s^{-1}$. Based on the obtained data, the height of current signals was reduced on the modified electrode with activated GO, and the peak separation was distinguished more precisely. This outcome could be due to the formation of insulative hydroxyl functional groups resulting from the decoration of an activated GO layer on the electrode's surface. However, the signal of the redox peak related to the $(Fe(CN)_6)^{3-/4-}$ was remarked upon introduction of Au NS to the composition owing to the inherent conductivity of Au NS, which facilitates the overall charge transfer rate within the solution [26]. EIS analyses were performed at a frequency ranging from 0.1 to 10^5 Hz toward assessing the overall performance of developed sensors in case of interfaces and conductivity [27]. The obtained results were in good agreement with CV measurements, as presented in Fig. 2 (b). The modified GCE with Au NSs showed a straight line with a low R_{ct} value of 21.53 Ω, showing a far better charge transfer rate due to Au NS's predominant electronic transferability. After that, by assessing the modified GCE with activated GO, the electrode indicated a higher resistance (R_{ct} of 1130 Ω), whereas, upon coating the GCE with G-Au NS platform, a relatively low R_{ct} with a small semicircle domain (R_{ct} = 83.6 Ω) was acquired. This remarkable change is appeared because of the unique features of Au NS as a superior electroactive nanomaterial. These data indicated that the G-Au NS platform significantly improved the electron transfer rate of bare GCE and proved to be an ideal modifying agent for working electrodes toward precise detection of SARS-CoV-2 antibody in biological fluids.

Additionally, developed nanomaterials' performance toward evaluating their antibody loading capability was also assessed through EIS and DPV analyses in PBS with pH 7.4; in Fig. 2, a view of these data can be seen clearly. As shown within Fig. 2 (c), the related EIS outcome for each modified GCE is approximated, and electron transfer kinetics parameters, including Rs, R_{ct}, and C_{dl}, were extracted and tabulated in Table 1. As tabulated, the initial value of C_{dl} for the bare GCE was considerably declined upon the decoration of GCE with activated GO and G-Au NS owing to coverage of active sites of GCE by compositions mentioned above, which could thence lead to an increase in the thickness of the final film. In this matter, the C_{dl} and C_{ϕ} parameters can be measured via the following formula:

$$Q = C^{g}(R_s^{-1} + R_{ct}^{-1})c^{1-g}$$

The “g” parameter, which indicates the surface inhomogeneity and the porosity of the surface, is close to unity upon the accumulation of antibodies on the active surface area of the electrode [28]. The surface concentration (r) of adsorbed antibodies on the modified GCE by G-Au NS can be estimated from the following equation [2]:

$$r_{DPV} = Q_{(DPV)}/nFA$$

where n is the electron transfer rate (in here the value is 1), F is the Faraday constant (96485.34 $C.mol^{-1}$), r is the surface concentration, and A is the surface area of the electrode. In this matter, the r value of IgG antibody against S1 protein of SARS-CoV-2 was measured to be 1.56 × 10^{-7} $mol.cm^{-2}$, indicating the successful absorption of

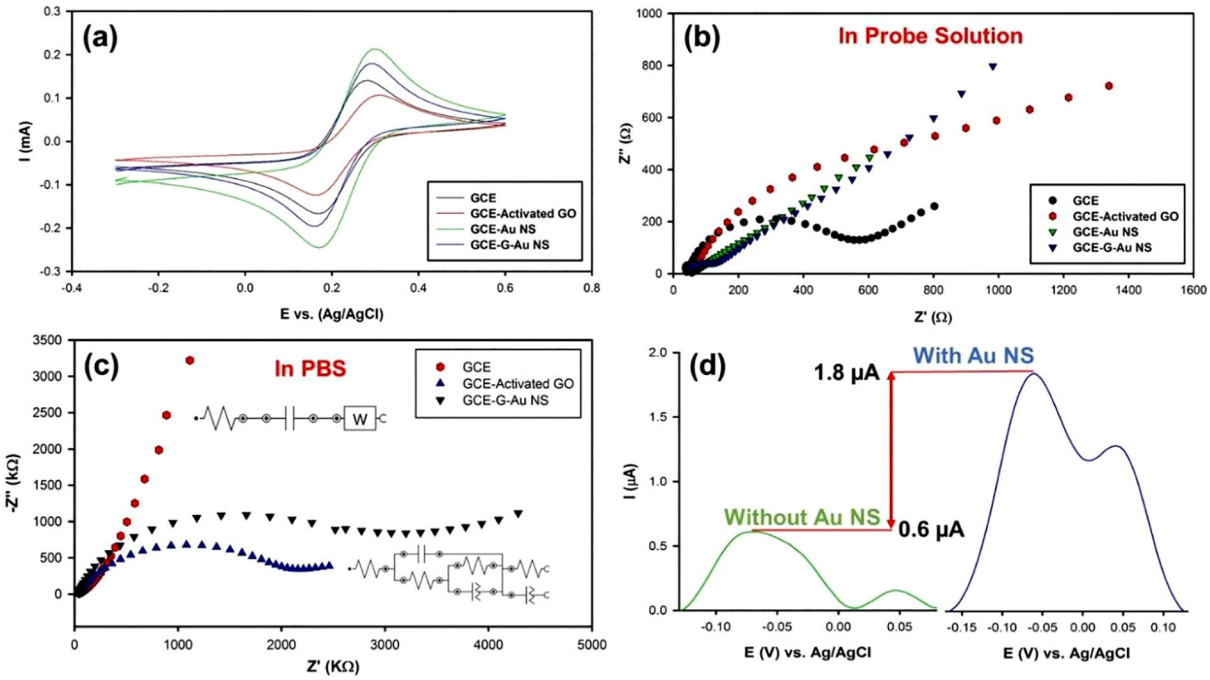

Fig. 2. (a) CV plots of developed compounds, (b) Nyquist plots of fabricated nanomaterials in probe solution, (c) EIS analysis of modified electrodes in the PBS (pH 7.4 and 0.1 M KCl) after absorption of antibody (insert shows related fit circuit) and (d) increase in the intensity of DPV analysis upon addition of Au NS to activated GO nanoflakes.

Table 1
Extracted electrochemical data from EIS analyses achieved from the GCE, activated GO and G-Au NS electrodes after absorption of antibody on their surfaces; all of the assessments were conducted in 0.1 M PBS with pH 7.4, without any external redox probe E_{DC} = +0.05 V (vs. Ag/AgCl).

Electrode	R_s (Ω)	R_{ct} (Ω)	C_{dl} (μF)	n
GCE	425 ± 3.2	–	1.6 ± 0.05	0.72
GCE-Activated GO	448 ± 2.2	120 ± 1	0.11 ± 0.01	0.81
GCE-G-Au NS	413 ± 1.4	254 ± 3	0.17 ± 0.01	0.95

the antibody with the modified GCE by G-Au NS. Moreover, as depicted in Fig. 2 (c) and Table 1, absorption of antibodies by both activated GO and G-Au NS modified electrodes led to a considerable increase in their overall R_{ct}, which is a piece of clear evidence for successful absorption of antibodies by the nanosensor and their attachment on the surface of the electrode that could subsequently lead to the generation of a unique electrochemical pattern for these antibodies in the DPV assay. Likewise, an increase in the R_{ct} of developed compounds after absorption of antibodies and generation of a semicircle pattern in their EIS plots vividly exhibit the successful attachment of antibodies to the surface of nanosensor via their electroactive $–NH_2$ functional groups located on the variable region of their light chains (Fig. 2 (c)).

In accord with EIS data, the DPV analysis confirmed the modified platform's superior performance toward detecting SARS-CoV-2 antibodies in PBS with pH 7.4. As shown in Fig. 2 (d), activated GO noticed the antibody with an intensity of 0.6 μA with a wider twin peak. Simultaneously, the addition of Au NSs to the composition considerably intensified the peak by about 200% and improved the pattern's quality. These data clearly showed the integrated nanosensor's fantastic performance toward accurate/direct detection of SARS-CoV-2 antibodies in biological fluids. They furtherly highlighted the amplifying role of Au NSs for better detection of IgG antibodies against S1 glycoprotein of SARS-CoV-2.

Additionally, the effect of potential scan rate (υ) on the electrochemical properties of GCE-G-Au NS between the range of 30–300 $mV.s^{-1}$ was studied by CV measurement in the probe solution (5 mM $Fe(CN)_6^{3-/4-}$) (Fig. S1). According to the Randles-Sevcik equation ($I_p = 2.69 \times 10^5\ n^{3/2}A_{eff}D^{1/2}\nu^{1/2}C$) and the slope of Ip-$\nu^{1/2}$ plot, the effective area of GCE-G-Au NS was estimated to be 5.24 mm^2, which is considerably higher than other electrodes. In the Randles-Sevcik equation, I_p is the current signal (A), n is electrons transfer rate, A_{eff} is the effective surface area (cm^2), D is the diffusion coefficient of 5.0 mM $K_3Fe(CN)_6$ ($cm^2.s^{-1}$), v is the scan rate ($V.s^{-1}$), and C is related to the bulk concentration of redox probe ($mol.mL^{-3}$).

GCE-G-Au NS platform's electrocatalytic capability regarding the rapid detection of monoclonal antibodies against S1 glycoprotein of SARS-CoV-2 in biological and non-biological fluids was initially traced by DPV technique in PBS with pH 7.4. In Fig. 3 (a), the fingerprint pattern of SARS-CoV-2 antibody from the concentration of 10^{-20} to 10^{-1} %V/V was evaluated. As clearly demonstrated within this Figure, monoclonal IgG antibody against S1 glycoprotein of SARS-CoV-2, viz., positive control of EUROIMMUN ELISA kit, showed a clear pattern with twin peaks between voltage range of −0.15 V to 0.15 V through the usage of the fixed three-electrode system. Accordingly, the first and second peaks appeared at −0.03 V and 0.06 V showing similar patterns to the S1 glycoprotein of SARS-CoV-2, as mentioned in our previous study [22]. Correspondingly, the monoclonal antibody against S1 glycoprotein of SARS-CoV-2 shows a very similar pattern compared with its source antigen and exhibits an electrochemical pattern with twin peaks at −0.02 V and 0.06 V between voltage range of −0.15 V to 0.15 V. This evidence confirmed the specific attachment of monoclonal antibody against S1 glycoprotein of SARS-CoV-2 antigen to the nanosensor owing to considerable similarities between their DPV patterns that could be due to the similarities in their active functional groups for effective immunological interaction between the antibody and source antigen.

In the next step, the quantitative analysis of antibody in PBS (pH 7.4) was conducted through the generation of differential pulse voltammograms of antibody through varying concentrations of antibody in the optimum assessment conditions; a view of these data can be seen in Fig. 3 (b), while their related calibration curve can be seen in Fig. S2(a). As can be seen, the current signals appeared at voltage positions of −0.03 V and 0.06 V and soared by a respective increase in the concentration of antibody on the surface of the electrode, which could be due to the excellent affinity of activated electrocatalyst toward protein structures and subsequent trapping of amino and acidic functional groups of protein compounds, which was more evident in the presence of G-Au NS as a catalytic mediator. Likewise, as can be seen in the insert of Fig. S2(a), the linear relationship between concentrations of antibody and peak currents can be expressed as $I_p = 0.16$ %V/V + 1.44 with R^2 of 0.9942, which shows a fantastic detection limit (DL, S/N = 3) and sensitivity (m/A) [29] of 0.097×10^{-19} %V/V and 5.11 μA.$(\%V/V)^{-1}.cm^{-2}$, respectively, at liner ranges of 0.25×10^{-19}-40×10^{-19} % V/V. Furthermore, it is worth mentioning that no peak was observed at the modified glassy carbon electrode with G-Au NS in the absence of antibody. The electrochemical characters of catalyst that lead to the detection of this typical structure could be related to the large surface area provided by GO nanoflakes and the great active functional groups provided by 8H, EDC and NHS, along with superior electrocatalytic activity/electrical conductivity of Au NSs. More importantly, the predominant tip in this issue could be attributed to the activation of amino/hydroxyl functional groups of nanocomposites upon introducing highly active EDC/NHS crosslinkers that can enhance the sensitivity of nanosensor.

To check the capability of the developed nanosensor toward detection of SARS-CoV-2 antibody in biological fluids, the DPV pattern of monoclonal antibody against S1 glycoprotein of SARS-CoV-2 (Fig. 3 (c)) and its related calibration curve were obtained in human blood plasma as aqueous biological sample (Fig. S2(b)). The calibration curve of monoclonal antibodies was obtained in the range of $1.25 \times 10^{-19} - 90 \times 10^{-19}$ %V/V, whereas the respective DL and sensitivity were estimated to be 0.18×10^{-19} % V/V and 2.14 μA.$(\%V/V)^{-1}.cm^{-2}$, respectively, for received current signals in human blood plasma samples. Obtained data vividly showed that the developed nanosensor based on the G-Au NS exhibits a very low DL and superiorly high sensitivity toward detecting monoclonal antibodies against S1 glycoprotein within aquatic media. What is more, the antibody also appeared at the same position in both PBS and plasma samples, viz., −0.03 and 0.06 V, which furtherly confirm the repeatability of the nanosensor's response.

The fantastic electrocatalytic performance of GCE-G-Au NS could be owing to the perfect adsorptive potential of activated GO in conjunction with Au NSs, in which the Au NS facilitates the overall electron transfer rate and the activated GO improves the specific active surface area and sensitivity of the integrated platform toward direct detection of S1 antibody through its electroactive functional groups. In this regard, the proposed electrocatalyst could provide more adsorptive ability for antibodies through diverse interactions, including hydrogen bonding between either amino or acidic functional groups of antibodies with active functional groups of nano electrocatalyst on the modified working electrode's surface.

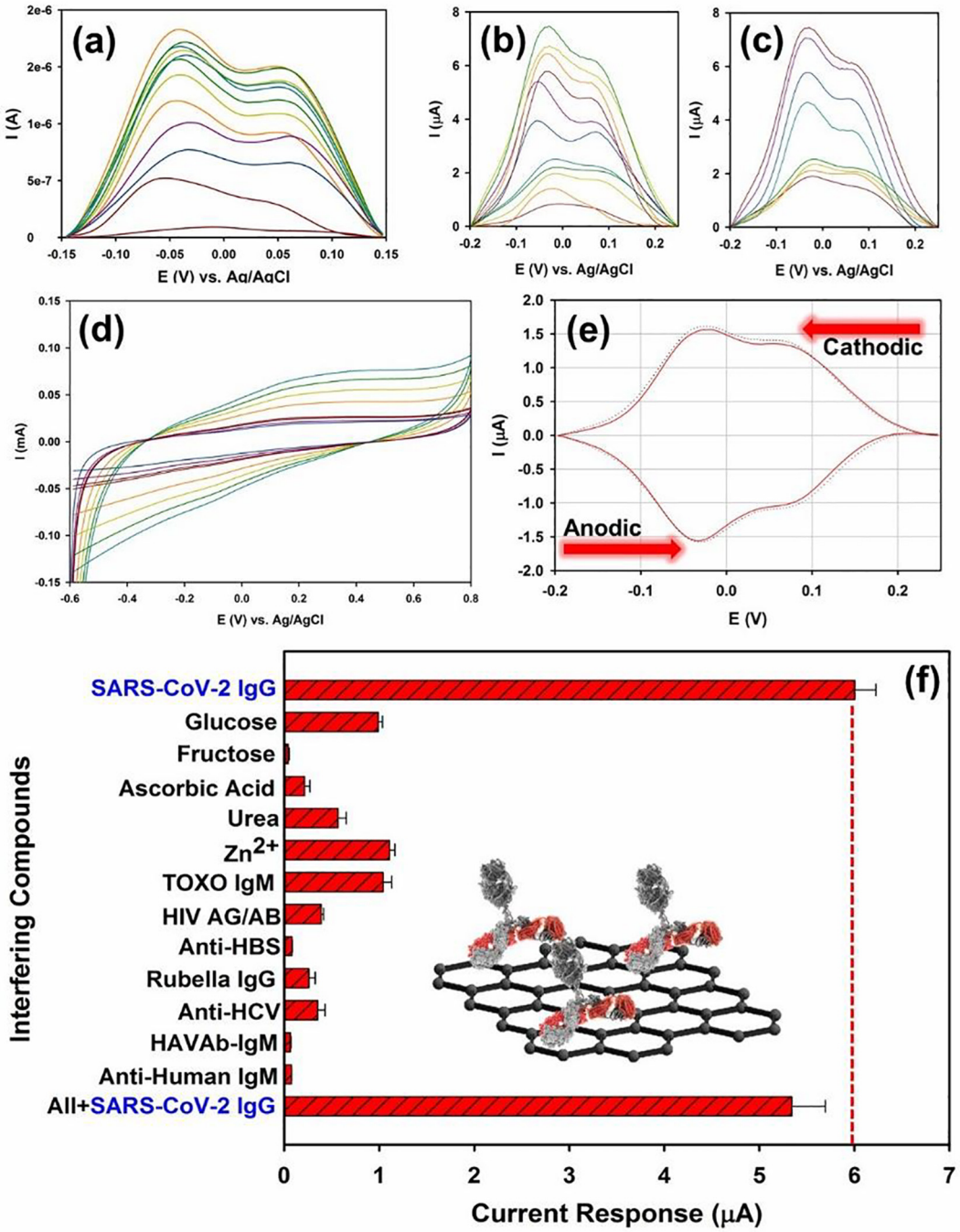

Fig. 3. (a) Fingerprint of monoclonal antibody against S1 glycoprotein of SARS-CoV-2 in PBS (pH 7.4) from the concentration of 10^{-20} to 10^{-1} %V/V, (b) detection of antibody against S1 in PBS (pH 7.4) from the concentration of 0.25 × 10^{-19} %V/V to 40 × 10^{-19} %V/V, (c) detection of antibody against S1 in the human blood plasma from the concentration of 1.25 × 10^{-19} %V/V to 90 × 10^{-19} %V/V, (d) CV scans of antibody against S1 with the scan rate ranging from 0.01 to 0.2 V.s^{-1}, (e) cathodic/anodic DPV pattern of antibody against S1 glycoprotein of SARS-CoV-2 and (f) effect of interfering compounds on the current signal of monoclonal antibodies.

In addition, CV analysis as one of the most practical and common assessment approaches for the characterization of selected chemical compounds could be employed as an efficient tool for examining electrochemical mechanisms of diverse chemical reactions. In this regard, the possible mechanism for adsorption of monoclonal antibody against S1 glycoprotein on the modified electrode's surface was initially assessed through CV analyses. To evaluate the proposed technique's electrocatalytic mechanism, the effect of variable potential scan rate on the electrochemical detection mechanism of antibodies was first performed via the CV method. As demonstrated within Fig. 3 (d), upon changing the scan rate from 0.01 to 0.2 V s^{-1}, a set of weak current signals were observed; the related calibration curve can also be seen in Fig. S2(c). Correspondingly, obtained data via variation of anodic currents over scan rates revealed that the reaction is controlled/governed via the surface-confined reactions and adsorption electron transfer mechanism on the active surface area of the working electrode, which exhibits that the process is based on the direct electron transfer mechanism.

Furthermore, due to the inherent low resolution and sensitivity of the CV method, it is more desired to utilize DPV as a far more sensitive

Table 2
The outcome of blind samples evaluation by the developed nanosensor compared with the ELISA kit as the gold standard with a cutoff point of 0.2 μA; (P: positive, N: negative).

Parameter	Formula	Obtained Percentage (%)
Sensitivity	TP/TP + FN	100
Specificity	TN/TN + FP	85
Negative prediction value	TN/TN + FN	100
Positive prediction value	TP/TP + FP	86.95
False-negative rate	FN/FN + TP	0
False-positive rate	FP/FP + TN	15
False discovery rate	FP/FP + TP	13.04
Accuracy	(TP + TN)/P + N	92.5
False-negative rate	FN/P	0
False-positive rate	FP/N	15

assay to improve the obtained results' resolution. Thereby, more accurate outcomes can be achieved by DPV analysis to recognize various mechanisms occurring on the electrode's surface. Accordingly, to probe the antibodies' detection mechanism against S1 glycoprotein, the forward and backward sweeping of potential related to the antibodies' voltammetric pattern was performed, and their respective current signals were carefully analyzed. Fig. 3 (e) exhibits the obtained processes related to the antibody against S1 glycoprotein within a PBS solution with pH 7.4. The labelled signal of the redox peak traced at the voltage position of −0.03 V is attributed to the nanosensor's electrochemical response on the modified working electrode's surface. The outcome of the DPV essay illustrated a slightly weak peak separation, somewhat about ~ 20 mV between the cathodic and anodic peaks, which showed ipa/ipc ~ 1, exhibiting a reversible process, and correspond to the adsorption and interaction of electroactive hydroxyl or amine functional groups of the monoclonal IgG antibody against S1 glycoprotein with NHS/EDC activated hydrogen-based groups on the surface of modified electrode. These outcomes clearly showed that the process is governed via the electrochemical (E) mechanism. What is more, the introduction of 8H to the composition could increase the total number of activated OH^- species. Meanwhile, the addition of the NHS/EDC complex to the activated GO could improve the absorption and subsequent interaction of IgG antibodies with the activated hydrogen-based functional groups by the NHS/EDC complex, which could thereby increase the possible hydrogen bonding at physiological pH value, i.e., 7.4. These modifiers could also improve the electrostatic interaction between active functional groups of antibodies and the nanosensor. Additionally, boosted redox reaction via Au NSs and interaction with its amine-based active functional groups could significantly improve the nanosensor's performance for precise/sensitive detection of monoclonal antibody against S1 glycoprotein in either biological or non-biological fluids.

Furthermore, the influence of diverse kinds of electroactive interference compounds such as Zn^{2+} ion, glucose, fructose, urea, ascorbic acid, the possible interfering antibodies related to various severe illness, viz., Hepatitis A (HAVAb IgM), Hepatitis B (anti-HBS), Hepatitis C (anti-HCV), HIV antigen (AG)/antibody (AB), Toxoplasmosis (Toxo IgM) and Rubella IgG, and anti-human IgM immunoglobulin on the electrochemical responses of 1.0×10^{-19} %V/V monoclonal antibodies against S1 glycoprotein of SARS-CoV-2 have been precisely assessed through pouring 0.1 mM of each interfering biomolecule, viz., fructose, ascorbic acid (AA), glucose, Zn^{2+}, urea, and 5×10^{-4} %V/V of each antibody in the electrolyte. Achieved results vividly showed that the selected interference compounds do not have any considerable effect on the I_p of monoclonal antibodies of SARS-CoV-2, which highlight the apparent ability of the nanosensor for accurate/specific detection of monoclonal antibodies against S1 glycoprotein of SARS-CoV-2 even upon the presence of a large amount of interferences compounds and antibodies related to other pathogens within the aquatic biological or non-biological media (Fig. 3 (f)).

To check the developed nanosensor's capability to accurately detect IgG antibodies against S1 proteins of SARS-CoV-2 within human blood plasma samples, 40 blind samples were selected containing 20 positive and 20 negative samples. These samples were first assessed via the EUROIMMUN anti-SARS-CoV-2 ELISA (IgG) kit, and achieved data were considered a reference for judging the developed nanosensor. A view of completed data and OD values of ELISA assays and the DPV fingerprint of antibodies is illustrated in Table S1. As tabulated, the developed nanosensor revealed a perfect agreement with obtained data from the ELISA assay. Accordingly, the nanosensor detected the fingerprint of antibody against S1 glycoprotein in 26 samples, while 14 samples did not show any pattern. By considering the cutoff point of 0.2 μA, the nanosensor exhibited 20 true positives (TP), 3 false positives (FP), 17 true negatives (TN) and 0 false negatives (FN) values; a complete evaluation of obtained outcomes by the nanosensor compared with the ELISA kit can be seen in Table 2. The nanosensor exhibited sensitivity and specificity of 100 and 85% at the cutoff point of 0.2 μA, which shows the developed platform's fantastic performance toward accurate/confident detection of antibodies in actual samples. More importantly, a follow-up of six patients out of 40, all of who the nanosensor detected the fingerprint pattern of IgG antibodies against S1 glycoprotein of SARS-COV-2 in their blood samples while the ELISA kit considered them as negative samples, showed that five of six patients had either clinical signs of COVID-19 or positive RT-PCR outcomes. This outcome vividly indicates the sensor's great potential in viral infections identification and covering the missing rate of common diagnostic platforms, i.e., ELISA or RT-PCR.

Furthermore, validation of achieved clinical data and correlation between the nanosensor and ELISA assay were assessed via plotting the related ROC curves (Fig. S3); accordingly, related evidence can be seen within Tables S2-S7. As demonstrated within Fig. S3 (a) and Tables S2 and S3, the developed nanosensor showed perfect outcomes with an area under the curve (AUC) of 0.995, standard error of 0.007 and lower bound/upper bound of 0.982/1.000, which revealed the superior accuracy of the sensor and compatibility of its outcomes with the obtained data from ELISA assay. Correspondingly, in Table S3, the relation between a cutoff point and sensitivity/specificity of the test can be seen. As tabulated, at a cutoff point of 0.2185 μA, the sensor showed a sensitivity/specificity of 100%/85%. In comparison, at a cutoff point of 0.3265 μA, the sensitivity/specificity becomes 95%/100%. Obtained outcomes vividly showed that the sensor could be used as a diagnostic kit for the confident evaluation of ill people with the infectious disease of COVID-19. These outcomes exhibit the platform's flexibility for becoming a fast diagnostic setup for either screening (at high sensitivities) or confident detection of viral disease (at high specificities).

What is more, in Fig. S3 (b) and Tables S4–S7, the correlation between the intensity of nanosensor based on μA and optical density obtained via ELISA assay was assessed. As demonstrated, the nanosensor showed a strong correlation with ELISA assay data with an AUC of 0.995, revealing the nanosensor's fantastic accuracy compared with the gold standard.

The detection mechanism of IgG antibodies by the nanosensor is also assessed to further highlight its label-free approach toward precise detection of antibodies. The developed nanosensor is perfectly beautified with exciting features that enable the rapid electrochemical detection of antibodies via their active functional groups. Accordingly, the GO provides wide active surface area along with active hydrophilic functional groups such as –OH and C═O that ease the interaction with considered modifiers and thereby lead to their homogeneous distribution and attachment throughout and on the surface of GO, respectively [29–32]. Moreover, the addition of 8H to the GO improves the overall rate of –OH functional groups and boosts the platform's sensitivity through its quinoline structure. More importantly, the addition of the NHS/EDC complex to the GO and 8H leads to activation of carbonyl and hydrogen-based functional groups that improve the interac-

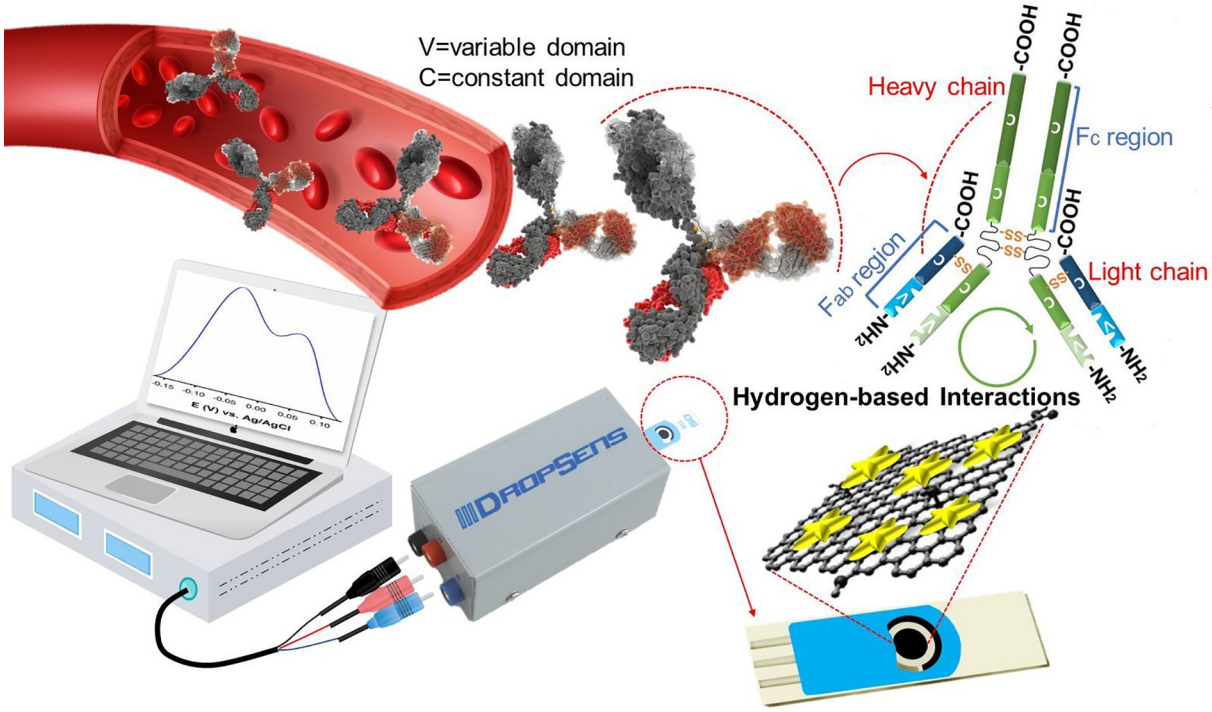

Fig. 4. Interaction of G-Au NS complex with IgG antibodies against S1 glycoprotein of SARS-CoV-2.

tion of the developed nanosensor with $–NH_2$, –OH and C═O functional groups and provides the possibility for efficient absorption of antibodies through their electroactive amine functional groups located on their F_{ab} region at neutral pH values. This process leads to the absorption of antibodies via the nanosensor and subsequent generation of a unique electrochemical pattern for IgG antibodies' glycoprotein structure via DPV assay. Additionally, the addition of Au NSs to the complex of activated GO improves the intensity of the nanosensor's voltammetric response, detection limit and sensitivity toward detection of antibodies, which arises from the superior electrical conductivity, electrocatalytic activity and compatibility of the Au NS with the graphene-based substrate [22]. In Fig. 4, a general view of this process can be seen.

3. Conclusion

Fast person-to-person transfer of pathogenic viruses such as SARS-CoV-2 throughout the world raised healthcare authorities' requirements for developing precise, rapid and sensitive diagnostic platforms capable of detecting SARS-CoV-2′s biomarkers within biological samples. In this study, we have addressed this urgent requirement via developing a quick, ultra-high sensitive and precise nanosystem based on integrated Au NS with an activated graphene-based platform that can rapidly detect the trace/fingerprint of monoclonal IgG antibody of SARS-CoV-2′s S1 protein within biological media with fantastic DL and sensitivity of 0.18×10^{-19} % V/V and 2.14 μA.$(\%V/V)^{-1}$. cm^{-2}, respectively. The sensor also exhibited a strong correlation with obtained data from gold-standard (ELISA assay). In this matter, it showed perfect sensitivity/specificity of about 100%/85% and 95%/100% at cutoff points of 0.2185 μA and 0.3265 μA, respectively, along with AUC of 0.995 from ROC curves. These outcomes justified the fantastic performance of the developed diagnostic kit for precise, rapid, and confident detection of infected people with the infectious disease of COVID-19, which is a vital requirement for viral outbreaks.

CRediT authorship contribution statement

Seyyed Alireza Hashemi: Conceptualization, Methodology, Software, Validation, Formal analysis, Investigation, Data Curation, Writing - original draft, Writing - review & editing, Visualization, Project administration. **Sonia Bahrani:** Conceptualization, Methodology, Software, Validation, Formal analysis, Investigation, Data Curation, Writing - original draft, Writing - review & editing. **Seyyed Mojtaba Mousavi:** Validation, Resources, Funding acquisition. **Navid Omidifar:** Conceptualization, Methodology, Validation, Formal analysis, Resources. **Nader Ghaleh Golab Behbahan:** Validation, Resources. **Mohammad Arjmand:** Conceptualization, Validation, Formal analysis, Resources, Data curation, Supervision. **Seeram Ramakrishna:** Validation, Supervision. **Kamran Bagheri Lankarani:** Validation, Supervision. **Mohsen Moghadami:** Conceptualization, Methodology. **Mansoureh Shokripour:** Methodology. **Mohammad Firoozsani:** Validation, Resources. **Wei-Hung Chiang:** Validation, Supervision.

Declaration of Competing Interest

The authors declare that they have no known competing financial interests or personal relationships that could have appeared to influence the work reported in this paper.

Acknowledgement

Full details of the experimental section and procedures are fleshed out within the supporting information section. Moreover, further details of nanosensor's characteristics and evaluation of actual samples and data of ROC curves are shown in the supporting information. Authentic samples assessment was carried out according to standard procedures by considering all of the required ethical issues. This project is also registered in the Shiraz University of Medical Sciences under the ethic code of IR.SUMS.REC.1399.1015. Additionally, this

project was conducted with the full financial and logistic support of Ebtekar Nano Sanat Kimia's scientific-based company located in the Shiraz Science and Technology Park, Shiraz, Iran and INVEX company located in Frankfort, Germany.

Appendix A. Supplementary data

Supplementary data to this article can be found online at https://doi.org/10.1016/j.jelechem.2021.115341.

References

[1] J. Cui, F. Li, Z.-L. Shi, Origin and evolution of pathogenic coronaviruses, Nat. Rev. Microbiol. 17 (3) (2019) 181–192.
[2] S. Su, G. Wong, W. Shi, J. Liu, A.C.K. Lai, J. Zhou, W. Liu, Y. Bi, G.F. Gao, Epidemiology, genetic recombination, and pathogenesis of coronaviruses, Trends Microbiol. 24 (6) (2016) 490–502.
[3] X. Zhu, X. Wang, L. Han, T. Chen, L. Wang, H. Li, S. Li, L. He, X. Fu, S. Chen, Reverse transcription loop-mediated isothermal amplification combined with nanoparticles-based biosensor for diagnosis of COVID-19, MedRxiv (2020).
[4] S.M. Mousavi, S.A. Hashemi, N. Parvin, A. Gholami, S. Ramakrishna, N. Omidifar, M. Moghadami, W.-H. Chiang, S. Mazraedoost, Recent biotechnological approaches for treatment of novel COVID-19: from bench to clinical trial, Drug Metab. Rev. (2020) 1–30.
[5] G.A. Lacatusu, C. Vasilescu, I.F. Mihai, F. Filip-Ciubotaru, A. Vata, C. Manciuc, Covid-19 and air conditioning-is there an environmental link?, Environ. Eng. Manage. J. (EEMJ) 19 (7) (2020) 1255–1260.
[6] R. Antiochia, Developments in biosensors for CoV detection and future trends, Biosens. Bioelectron. 173 (2021) 112777, https://doi.org/10.1016/j.bios.2020.112777.
[7] J.C. Huang, Y.-F. Chang, K.-H. Chen, L.-C. Su, C.-W. Lee, C.-C. Chen, Y.-M. Chen, C. Chou, Detection of severe acute respiratory syndrome (SARS) coronavirus nucleocapsid protein in human serum using a localized surface plasmon coupled fluorescence fiber-optic biosensor, Biosens. Bioelectron. 25 (2) (2009) 320–325.
[8] N. Chen, M. Zhou, X. Dong, J. Qu, F. Gong, Y. Han, Y. Qiu, J. Wang, Y. Liu, Y. Wei, Epidemiological and clinical characteristics of 99 cases of 2019 novel coronavirus pneumonia in Wuhan, China: a descriptive study, Lancet 395 (10223) (2020) 507–513.
[9] P. Boraschi, COVID-19 pulmonary involvement: is really an interstitial pneumonia?, Acad. Radiol. 27 (6) (2020) 900, https://doi.org/10.1016/j.acra.2020.04.010.
[10] W.H. Organization, WHO Director-General's opening remarks at the media briefing on COVID-19-11 March 2020, 2020.
[11] N. Boonham, J. Kreuze, S. Winter, R. van der Vlugt, J. Bergervoet, J. Tomlinson, R. Mumford, Methods in virus diagnostics: from ELISA to next generation sequencing, Virus Res. 186 (2014) 20–31.
[12] T. Ozer, B.J. Geiss, C.S. Henry, Chemical and Biological Sensors for Viral Detection, J. Electrochem. Soc. 167 (3) (2019) 037523.
[13] L. Krejcova, P. Michalek, M.M. Rodrigo, Z. Heger, S. Krizkova, M. Vaculovicova, D. Hynek, V. Adam, R. Kizek, Nanoscale virus biosensors: state of the art, Nanobiosensors Dis. Diagn. 4 (2015) 47–66.
[14] A. Kawamura, T. Miyata, Biosensors, Biomaterials Nanoarchitectonics, Elsevier, 2016, pp. 157–176.
[15] G. Seo, G. Lee, M.J. Kim, S.-H. Baek, M. Choi, K.B. Ku, C.-S. Lee, S. Jun, D. Park, H. G. Kim, S.-J. Kim, J.-O. Lee, B.T. Kim, E.C. Park, S.I. Kim, Rapid detection of COVID-19 causative virus (SARS-CoV-2) in human nasopharyngeal swab specimens using field-effect transistor-based biosensor, ACS Nano 14 (4) (2020) 5135–5142.
[16] M.Z. Rashed, J.A. Kopechek, M.C. Priddy, K.T. Hamorsky, K.E. Palmer, N. Mittal, J. Valdez, J. Flynn, S.J. Williams, Rapid detection of SARS-CoV-2 antibodies using electrochemical impedance-based detector, Biosens. Bioelectron. 171 (2020) 112709.
[17] J.-H. Lee, M. Choi, Y. Jung, S.K. Lee, C.-S. Lee, J. Kim, J. Kim, N.H. Kim, B.-T. Kim, H.G. Kim, A novel rapid detection for SARS-CoV-2 spike 1 antigens using human angiotensin converting enzyme 2 (ACE2), Biosens. Bioelectron. 171 (2020) 112715.
[18] H. Zhao, F. Liu, W. Xie, T.-C. Zhou, J. OuYang, L. Jin, H. Li, C.-Y. Zhao, L. Zhang, J. Wei, Ultrasensitive supersandwich-type electrochemical sensor for SARS-CoV-2 from the infected COVID-19 patients using a smartphone, Sens. Actuators, B 327 (2020) 128899.
[19] Z.S. Miripour, R. Sarrami-Forooshani, H. Sanati, J. Makarem, M.S. Taheri, F. Shojaeian, A.H. Eskafi, F. Abbasvandi, N. Namdar, H. Ghafari, Real-time diagnosis of reactive oxygen species (ROS) in fresh sputum by electrochemical tracing; correlation between COVID-19 and viral-induced ROS in lung/respiratory epithelium during this pandemic, Biosens. Bioelectron. 165 (2020) 112435.
[20] L. Fabiani, M. Saroglia, G. Galatà, R. De Santis, S. Fillo, V. Luca, G. Faggioni, N. D'Amore, E. Regalbuto, P. Salvatori, Magnetic beads combined with carbon black-based screen-printed electrodes for COVID-19: A reliable and miniaturized electrochemical immunosensor for SARS-CoV-2 detection in saliva, Biosens. Bioelectron. 171 (2020) 112686.
[21] R.M. Torrente-Rodríguez, H. Lukas, J. Tu, J. Min, Y. Yang, C. Xu, H.B. Rossiter, W. Gao, SARS-CoV-2 RapidPlex: A Graphene-Based Multiplexed Telemedicine Platform for Rapid and Low-Cost COVID-19 Diagnosis and Monitoring, Matter 3 (6) (2020) 1981–1998.
[22] S.A. Hashemi, N.G.G. Behbahan, S. Bahrani, S.M. Mousavi, A. Gholami, S. Ramakrishna, M. Firoozsani, M. Moghadami, K.B. Lankarani, N. Omidifar, Ultra-sensitive viral glycoprotein detection NanoSystem toward accurate tracing SARS-CoV-2 in biological/non-biological media, Biosens. Bioelectron. 171 (2020) 112731.
[23] S.A. Hashemi, S.M. Mousavi, R. Faghihi, M. Arjmand, M. Rahsepar, S. Bahrani, S. Ramakrishna, C.W. Lai, Superior X-ray Radiation Shielding Effectiveness of Biocompatible Polyaniline Reinforced with Hybrid Graphene Oxide-Iron Tungsten Nitride Flakes, Polymers 12 (6) (2020) 1407.
[24] S.A. Hashemi, S.M. Mousavi, R. Faghihi, M. Arjmand, S. Sina, A.M. Amani, Lead oxide-decorated graphene oxide/epoxy composite towards X-Ray radiation shielding, Radiat. Phys. Chem. 146 (2018) 77–85.
[25] S.A. Hashemi, N.G. Golab Behbahan, S. Bahrani, S.M. Mousavi, A. Gholami, S. Ramakrishna, M. Firoozsani, M. Moghadami, K.B. Lankarani, N. Omidifar, Ultra-sensitive viral glycoprotein detection NanoSystem toward accurate tracing SARS-CoV-2 in biological/non-biological media, Biosens. Bioelectron. 171 (2020) 112731.
[26] S. Bahrani, Z. Razmi, M. Ghaedi, A. Asfaram, H. Javadian, Ultrasound-accelerated synthesis of gold nanoparticles modified choline chloride functionalized graphene oxide as a novel sensitive bioelectrochemical sensor: Optimized meloxicam detection using CCD-RSM design and application for human plasma sample, Ultrason. Sonochem. 42 (2018) 776–786.
[27] R. Karimi Shervedani, S. Bahrani, M. Samiei Foroushani, F. Momenbeik, Selective Detection of Dopamine in the Presence of Ascorbic and Uric Acids through its Covalent Immobilization on Gold Mercaptopropionic Acid Self-assembled Monolayer, Electroanalysis 29 (1) (2017) 272–279.
[28] R. Karimi Shervedani, M. Samiei Foroushani, S. Bagheri Dehaghi, Functionalization of gold mercaptopropionic acid self-assembled monolayer with 5-amino-1,10-phenanthroline: Interaction with iron(II) and application for selective recognition of guanine, Electrochim. Acta 164 (2015) 344–352.
[29] S.A. Hashemi, S.M. Mousavi, S. Bahrani, S. Ramakrishna, A. Babapoor, W.-H. Chiang, Coupled graphene oxide with hybrid metallic nanoparticles as potential electrochemical biosensors for precise detection of ascorbic acid within blood, Anal. Chim. Acta 1107 (2020) 183–192.
[30] S. Alireza Hashemi, S. Mojtaba Mousavi, H. Reza Naderi, S. Bahrani, M. Arjmand, A. Hagfeldt, W.-H. Chiang, S. Ramakrishna, Reinforced Polypyrrole with 2D Graphene Flakes Decorated with Interconnected Nickel-Tungsten Metal Oxide Complex Toward Superiorly Stable Supercapacitor, Chem. Eng. J. 418 (2021) 129396, https://doi.org/10.1016/j.cej.2021.129396.
[31] S.M. Mousavi, S. Soroshnia, S.A. Hashemi, A. Babapoor, Y. Ghasemi, A. Savardashtaki, A.M. Amani, Graphene nano-ribbon based high potential and efficiency for DNA, cancer therapy and drug delivery applications, Drug Metab. Rev. 51 (1) (2019) 91–104.
[32] R. Azhdari, S.M. Mousavi, S.A. Hashemi, S. Bahrani, S. Ramakrishna, Decorated graphene with aluminum fumarate metal organic framework as a superior non-toxic agent for efficient removal of Congo Red dye from wastewater, J. Environ. Chem. Eng. 7 (6) (2019) 103437, https://doi.org/10.1016/j.jece:2019.103437.